



1 Large carbon cycle sensitivities to climate across a permafrost thaw gradient in subarctic

2 Sweden

3

4 Kuang-Yu Chang\*,

5 Climate and Ecosystem Sciences Division, Lawrence Berkeley National Laboratory,

6 Berkeley, California, USA

7 William J. Riley,

8 Climate and Ecosystem Sciences Division, Lawrence Berkeley National Laboratory,

9 Berkeley, California, USA

10 Patrick Crill,

11 Department of Geological Sciences, Stockholm University, Stockholm, Sweden

12 Robert F. Grant,

13 Department of Renewable Resources, University of Alberta, Edmonton, Alberta, Canada

14 Virginia Rich,

15 Department of Microbiology, The Ohio State University, Columbus, Ohio, USA

16 and,

17 Scott Saleska,

18 Department of Ecology and Evolutionary Biology, University of Arizona, Tucson,

19 Arizona, USA

20

21

22 \*Corresponding author: Kuang-Yu Chang, [ckychang@lbl.gov](mailto:ckychang@lbl.gov)

23 Climate and Ecosystem Sciences Division, Lawrence Berkeley National Laboratory

24 Berkeley, California, USA

The Cryosphere Discuss., <https://doi.org/10.5194/tc-2018-215>  
Manuscript under review for journal The Cryosphere  
Discussion started: 17 October 2018  
© Author(s) 2018. CC BY 4.0 License.



25 Phone: (510) 495-8141



26 Abstract

27 Permafrost peatlands store large amounts of carbon potentially vulnerable to

28 decomposition. However, the fate of that carbon in a changing climate remains uncertain

29 in models due to complex interactions among hydrological, biogeochemical, microbial,

30 and plant processes. In this study, we estimated effects of climate forcing biases present

31 in global climate reanalysis products on carbon cycle predictions at a thawing permafrost

32 peatland in subarctic Sweden. The analysis was conducted with a comprehensive

33 biogeochemical model (*ecosys*) across a permafrost thaw gradient encompassing intact

34 palsa with an ice core and a shallow active layer, partly thawed bog with a deeper active

35 layer and a variable water table, and fully thawed fen with a water table close to the

36 surface, each with distinct vegetation and microbiota. Using *in situ* observations to

37 correct local cold and wet biases found in the Global Soil Wetness Project Phase 3

38 (GSWP3) climate reanalysis forcing, we evaluated our model performance by comparing

39 predicted and observed carbon dioxide (CO<sub>2</sub>) and methane (CH<sub>4</sub>) exchanges, thaw depth,

40 and water table depth. The simulations driven by the bias-corrected climate suggest that

41 the three peatland types currently accumulate carbon from the atmosphere, although the

42 bog and fen sites can have annual positive radiative forcing impacts due to their higher

43 CH<sub>4</sub> emissions. Our simulations indicate that projected precipitation increases could

44 accelerate CH<sub>4</sub> emissions from the palsa area, even without further degradation of palsa

45 permafrost. The GSWP3 cold and wet biases for this site significantly alter simulation

46 results and lead to erroneous active layer depth and carbon budget estimates. Biases in

47 simulated CO<sub>2</sub> and CH<sub>4</sub> exchanges from biased climate forcing are as large as those

48 among the thaw stages themselves at a landscape scale across the examined permafrost



49 thaw gradient. Future studies should thus not only focus on changes in carbon budget  
50 associated with morphological changes in thawing permafrost, but also recognize the  
51 effects of climate forcing uncertainty on carbon cycling.



## 52 **1. Introduction**

53 Confidence in future climate projections depends on the accuracy of terrestrial  
54 carbon budget estimates, which are presently very uncertain (Friedlingstein et al., 2014;  
55 Arneeth et al., 2017). In addition to the complexity in physical process representations, a  
56 major source of this uncertainty comes from challenges in quantifying climate responses  
57 induced by biogeochemical feedbacks. Increases in atmospheric carbon dioxide (CO<sub>2</sub>)  
58 concentrations can directly stimulate carbon sequestration from plant photosynthesis  
59 (Cox et al., 2000; Friedlingstein et al., 2006) and indirectly stimulate carbon emissions  
60 (e.g., from soil warming and resulting increased respiration), although the predicted  
61 magnitudes of these exchanges strongly depend on model process representations (Zaehle  
62 et al., 2010; Grant, 2013, 2014; Ghimire et al., 2016; Chang et al., 2018).

63 The undecomposed carbon stored in permafrost is of critical importance for  
64 biogeochemical feedbacks to climate because it is about twice as much as currently is in  
65 the atmosphere (Hugelius et al., 2014) and is vulnerable to release to the atmosphere as  
66 permafrost thaws (Schuur et al., 2015). Lundin et al. (2016) reported that it is plausible  
67 (71% probability) for the high latitude terrestrial landscape to serve as a net carbon  
68 source to the atmosphere, although its peatland components would remain atmospheric  
69 carbon sinks.

70 In addition to the overall carbon balance of the changing Arctic, the type of  
71 carbon gaseous emission is important to climate feedbacks. High latitudes are predicted  
72 to get wetter (IPCC, 2014), and saturated anaerobic conditions facilitate methane (CH<sub>4</sub>)  
73 production, which is a much more efficient greenhouse gas than CO<sub>2</sub> in terms of global  
74 warming potential. Even habitats that can be net carbon sinks can produce positive



75 radiative forcing impacts on climate due to CH<sub>4</sub> release, as Bäckstrand et al. (2010)  
76 showed for a subarctic peatland. Under projected warming and wetting trends in the  
77 Arctic (Collins et al., 2013; Bintanja and Andry, 2017), carbon cycle feedbacks over the  
78 permafrost region could become stronger as increased precipitation enhances surface  
79 permafrost thaw and strengthens CH<sub>4</sub> emissions by expansion of anaerobic volume  
80 (Christensen et al., 2004; Wickland et al., 2006).

81 The Stordalen Mire in northern Sweden (68.20°N, 19.05°E) is in the  
82 discontinuous permafrost zone, encompassing a mosaic of thaw stages with associated  
83 distinct hydrology and vegetation (Christensen et al. 2004; Malmer et al., 2005),  
84 microbiota (Mondav and Woodcroft et al., 2014; Mondav et al., 2017; Woodcroft and  
85 Singleton et al., 2018), and organic matter chemistry (Hodgkins et al., 2014). These  
86 landscapes have been shifting over the last half-century to a more thawed state, likely due  
87 to recent warming (Christensen et al. 2004). Drier hummock sites dominated by shrubs  
88 have degraded to wetter sites dominated by graminoids (Malmer et al., 2005; Johansson  
89 et al., 2006). The thaw-induced habitat shifts are associated with increases in landscape  
90 scale CH<sub>4</sub> emissions (Christensen et al. 2004; Johansson et al., 2006; Cooper et al., 2017)  
91 reflective of the higher CH<sub>4</sub> emissions of the wetter thawed habitats (McCalley et al.,  
92 2014). The higher CO<sub>2</sub> uptake in later thaw-stage habitats has not compensated for the  
93 increase in positive radiative forcing from elevated CH<sub>4</sub> emissions (Bäckstrand et al.,  
94 2010; Deng et al., 2014).

95 The impacts of climate sensitivity on the terrestrial carbon cycle have been  
96 investigated at the global scale, and the results highlight the need to consider uncertainty  
97 in climate datasets when evaluating permafrost region carbon cycle simulations



98 (Ahlström et al., 2017; Guo et al., 2017; Wu et al., 2017). Ahlström et al. (2017) showed  
99 that climate forcing biases are responsible for a considerable fraction (~40%) of the  
100 uncertainty range in ecosystem carbon predictions from 18 Earth System Models (ESMs)  
101 reported by Anav et al. (2013). Guo et al. (2017) concluded that the differences in climate  
102 forcing contribute to significant differences in simulated soil temperature, permafrost  
103 area, and active layer thickness. Wu et al. (2017) demonstrated that differences among  
104 climate forcing datasets contributes more to predictive uncertainty than differences in  
105 apparent model sensitivity to climate forcing. However, notably, none of these studies  
106 accessed the effects on CH<sub>4</sub> emissions, and their spatial resolution could not represent  
107 site-level spatial heterogeneity observed in arctic tundra (Grant et al. 2017a; 2017b).

108         Here, we use the ecosystem model *ecosys*, which employs a comprehensive set of  
109 fully coupled biogeochemical and hydrological processes, to estimate the effects of  
110 climate forcing uncertainty and sensitivity on CO<sub>2</sub> and CH<sub>4</sub> exchanges and active layer  
111 thickness simulations. For the Stordalen Mire site, we estimated bias in the Global Soil  
112 Wetness Project Phase 3 (GSWP3) climate reanalysis dataset using site-level long-term  
113 meteorological measurements and evaluated impacts on simulated soil and plant  
114 processes across the permafrost thaw gradient. This approach enables us to assess model  
115 sensitivity to individual climate forcing biases, instead of the aggregated uncertainty  
116 range embedded in climate datasets (e.g., variations of climate conditions represented in  
117 different climate datasets) presented in previous studies. We address the following  
118 questions for our study site at the Stordalen Mire: (1) What are the biases embedded in  
119 the GSWP3 climate reanalysis dataset? (2) How do those biases affect model predictions  
120 of active layer depth, CO<sub>2</sub> exchanges, and CH<sub>4</sub> exchanges? (3) How does climate



121 sensitivity vary across the stages of permafrost thaw? In addition to improving  
122 understanding of permafrost responses to climate, we identify ecosystem carbon  
123 prediction uncertainty induced by climate forcing uncertainty in general as the biases  
124 found in GSWP3 were consistent with other climate reanalysis datasets during the last  
125 decade (section 3).

126

## 127 **2. Methods and Data**

### 128 **2.1 Study site description**

129 Our study sites are located at the Stordalen Mire (68.20 °N, 19.03 °E: 351 m  
130 above sea level), which is about 10 km southeast of the Abisko Scientific Research  
131 Station (ANS) in northern Sweden. Significant changes in climate over this region have  
132 been recorded during the last few decades. The annual mean air temperature measured at  
133 the ANS has risen by 2.5 °C from 1913 to 2006, where it exceeded the 0 °C threshold  
134 (0.6 °C in 2006) for the first time over the past century (Callaghan et al., 2010). The  
135 measured annual total precipitation has also increased from 306 mm y<sup>-1</sup> (years 1913 to  
136 2009) to 336 mm y<sup>-1</sup> (years 1980 to 2009) (Olefeldt and Roulet, 2012), along with  
137 increased variability in extreme precipitation (Callaghan et al., 2010). The measured  
138 annual maximum snow depth has increased from 59 cm (years 1957 to 1971) to 70 cm  
139 (years 1986 to 2000), and the snow cover period with snow depth greater than 20 cm has  
140 decreased from 5.8 months (years 1957 to 1971) to 4.9 months (years 1986 to 2000)  
141 (Malmer et al., 2005).

142 The Stordalen Mire can be broadly classified into three peatland types: intact  
143 permafrost palsa, partly thawed bog, and fully thawed fen (Hodgkins et al., 2014),



144 hereafter referred to as palsa, bog, and fen. The spatial distribution of these peatland  
145 types in 2000 can be found in Olefeldt and Roulet (2012). The palsa sites are  
146 ombrotrophic and raised 0.5 to 2.0 m above their surroundings, with a relatively thin peat  
147 layer (0.4 to 0.7 m, Rydén et al., 1980), thinner active layer depth (less than 0.7 m in late  
148 summer), and no measurable water table depth (Bäckstrand et al., 2008a; 2008b; Olefeldt  
149 and Roulet, 2012). The bog sites are ombrotrophic and are wetter than the palsa sites,  
150 with a thicker peat layer (0.5 to ~1 m, Rydén et al., 1980), thicker active layer depth  
151 (ALD) (greater than 0.9 m), and water table depth fluctuating from 35 cm to the ground  
152 surface (Bäckstrand et al., 2008a; 2008b; Olefeldt and Roulet, 2012). The fen sites have  
153 no permafrost and are minerotrophic, receiving a large amount of water from a lake to the  
154 east of the mire, with water table depths near or above the ground surface (Bäckstrand et  
155 al., 2008a; 2008b; Olefeldt and Roulet, 2012).

156 Differences in hydrology and permafrost conditions create high spatial  
157 heterogeneity with different soil moisture, pH, and nutrient conditions that support  
158 different plant communities (Bäckstrand et al., 2008a; 2008b). The palsa is dominated by  
159 dwarf shrubs with some sedges, feather mosses, and lichens (Malmer et al., 2005;  
160 Bäckstrand et al., 2008a; 2008b; Olefeldt and Roulet, 2012). The bog is dominated by  
161 Sphagnum spp. mosses with a moderate abundance of sedges (Malmer et al., 2005;  
162 Bäckstrand et al., 2008a; 2008b; Olefeldt and Roulet, 2012). The fen sites we studied are  
163 dominated by sedges (Bäckstrand et al., 2008a; 2008b).

164

## 165 **2.2 Field measurements**



166           Continuous daily meteorological measurements have been recorded at the ANS  
167   since 1913, including air temperature, precipitation, wind speed, wind direction, relative  
168   humidity, and snow depth. Measurements of solar radiation, longwave radiation, and soil  
169   temperature are also available at the ANS since 1982. The soil thaw depth (measured to  
170   90 cm) and water table depth measurements were taken in the three peatland types 3 to 5  
171   times per week from early May to mid-October during 2003 to 2007 (Bäckstrand et al.,  
172   2008b).

173           CO<sub>2</sub> and CH<sub>4</sub> exchanges at the three peatland types were measured with  
174   automated chambers during the thawed seasons from 2002 to 2007. Chamber lids were  
175   removed in the Fall and replaced in the Spring. Three chambers were in the palsa, three  
176   were in the bog, and two were in the fen. Each chamber covered an area of 0.14 m<sup>2</sup> with a  
177   height of 25–45 cm depending on the vegetation and the depth of insertion. Each  
178   chamber was closed for 5 minutes every 3 hours to measure CO<sub>2</sub> and total hydrocarbon  
179   (THC) exchanges. CH<sub>4</sub> exchanges were manually observed approximately 3 times per  
180   week, and these measurements were used to quantify the proportion of CH<sub>4</sub> in the  
181   measured THC (Bäckstrand et al., 2008a). The CH<sub>4</sub> exchanges were near zero in the  
182   palsa sites (Bäckstrand et al., 2008a; Bäckstrand et al., 2008b; Bäckstrand et al., 2010), so  
183   it was not incorporated in our model evaluation. We used the CO<sub>2</sub> and CH<sub>4</sub> exchanges  
184   observed at 3-hourly steps when the R<sup>2</sup> values recorded in the measurements were greater  
185   than 0.8 (Tokida et al., 2007), and then calculated the associated daily mean exchanges  
186   when there were 8 measurements per day (Table 1). The quality-controlled daily  
187   measurements only covered 12.4–33.7% of the daily data points because of the lack of  
188   continuous quality-controlled 3-hourly measurements. The data screening was applied to



189 exclude unreliable measurements and avoid biases from inappropriate gap filling, which  
190 is necessary for model evaluations. More detailed descriptions of the CO<sub>2</sub> and CH<sub>4</sub>  
191 exchanges measurements can be found in Bäckstrand et al. (2008a).

192

### 193 **2.3 GSWP3**

194 GSWP3 is an ongoing modeling activity that provides global gridded  
195 meteorological forcing (0.5° x 0.5° resolution) and investigates changes in energy-water-  
196 carbon cycles throughout the 20<sup>th</sup> and 21<sup>st</sup> centuries. The GSWP3 dataset is based on the  
197 20<sup>th</sup> Century Reanalysis (Compo et al., 2011), using a spectral nudging dynamical  
198 downscaling technique described in Yoshimura and Kanamitsu (2008). A more detailed  
199 description of the GSWP can be found in Dirmeyer (2011) and van den Hurk et al.  
200 (2016).

201 In this study, we extracted the meteorological conditions at the Stordalen Mire  
202 from 1901 to 2010 from the GSWP3 climate reanalysis dataset. The 3-hourly products of  
203 air temperature, precipitation, solar radiation, wind speed, and specific humidity were  
204 interpolated to hourly intervals with cubic spline interpolation to serve as the  
205 meteorological inputs used in our model.

206 The GSWP3 dataset was chosen over other existing climate reanalysis datasets for  
207 its spatial and temporal resolutions. For example, the Climatic Research Unit (CRU;  
208 Harris et al., 2014) dataset provided monthly meteorological forcing at 0.5° x 0.5°  
209 resolution; the National Centers for Environmental Prediction (NCEP; Kalnay et al.,  
210 1996; Kanamitsu et al., 2002) dataset provided 6-hourly meteorological forcing at T62  
211 Gaussian grid (~1.915° x 1.895° resolution); the CRUNCEP (Viovy, 2018) dataset



212 provided 6-hourly meteorological forcing at  $0.5^\circ \times 0.5^\circ$  resolution; and the European  
213 Centre for Medium-Range Weather Forecasts (ECMWF; Berrisford et al., 2011) dataset  
214 provided 3-hourly meteorological forcing with 125 km ( $\sim 1.125^\circ$ ) horizontal resolution.

215

## 216 **2.4 Model description**

217 *Ecosys* is a comprehensive biogeochemistry model that simulates ecosystem  
218 responses to diverse environmental conditions with explicit representations of microbial  
219 dynamics and soil carbon, nitrogen, and phosphorus biogeochemistry. The above-ground  
220 processes are represented in multi-layer plant interacting canopies, and the below-ground  
221 processes are represented in multiple soil layers with multi-phase subsurface reactive  
222 transport. *Ecosys* operates at variable time steps (down to seconds) determined by  
223 convergence criteria, and it can be applied at patch scale (spatially homogenous one-  
224 dimensional) and landscape scale (spatially variable two- or three-dimensional). Detailed  
225 descriptions, including inputs, outputs, governing equations, parameters, and references  
226 of the *ecosys* model can be found in Grant (2013).

227 The *ecosys* model has been extensively tested against eddy covariance fluxes and  
228 related ecophysiological measurements with a wide range of sites and weather conditions  
229 in boreal, temperate, and tropical forests (Grant et al., 2007a; Grant et al., 2007c; Grant et  
230 al., 2009a; Grant et al., 2009b; Grant et al., 2009c; Grant et al., 2010), wetlands (Dimitrov  
231 et al., 2011; Grant et al., 2012b; Dimitrov et al., 2014; Mezbahuddin et al., 2014),  
232 grasslands (Grant and Flanagan, 2007; Grant et al., 2012a), tundra (Grant et al., 2003;  
233 Grant et al., 2011b; Grant 2015; Grant et al., 2015), croplands (Grant et al., 2007b; Grant  
234 et al., 2011a), and other permafrost-associated habitats (Grant and Roulet, 2002; Grant,



235 2017a; Grant et al., 2017b). All *ecosys* model structures are unchanged from those  
236 described in these earlier studies.

## 237 **2.5 Experimental design**

238 To evaluate the effects of climate on model predictions, we conducted four sets of  
239 simulations at each of the three peatland types at the Stordalen Mire from 1901 to 2010.  
240 The 110 year simulations were performed to ensure the simulation was equilibrated with  
241 local climate (Grant et al. 2017a).

242 The meteorological conditions for all the simulations were based on the hourly  
243 data extracted from the GSWP3 climate reanalysis dataset (section 2.3). The monthly  
244 mean bias of the GSWP3 for this location was calculated by comparing it to the air  
245 temperature and precipitation measured at the ANS, for years 1913 to 2010 (section 3.1).  
246 The full series of air temperature and precipitation extracted from GSWP3 were then  
247 bias-corrected using the monthly mean bias calculated from 1913 to 2010; we label this  
248 model scenario CTRL. Our bias correction was conceptually similar to the one used in  
249 Ahlström et al. (2017), where the bias-corrected climate forcing fields were the ESM  
250 outputs adjusted by the corresponding bias calculated from observations in a reference  
251 period.

252 The simulation results from CTRL should represent the reliability of applying  
253 *ecosys* at the Stordalen Mire because CTRL is driven by the best local climate  
254 description. We first evaluated predicted thaw depth, water table depth, and CO<sub>2</sub> and CH<sub>4</sub>  
255 exchanges using the CTRL simulation (section 3.2 to 3.4). In the second set of  
256 simulations, BIASED-COLD, the biased GSWP3 air temperature data was used, and we  
257 corrected only the GSWP3 precipitation. Deviations between CTRL and BIASED-COLD



258 reflect biased air temperature's effects on responses across the thaw gradient. In the third  
259 set of simulations, BIASED-WET, we bias-corrected the air temperature extracted from  
260 GSWP3, which allows us to quantify the effects of biased precipitation. Finally, we used  
261 the meteorological conditions directly extracted from GSWP3 to drive our fourth set of  
262 simulations, BIASED-COLD&BIASED-WET, which reveals the uncertainty range of  
263 subarctic peatland simulation associated with the local biases in GSWP3 climate forcing.

264 While the three peatland types share the same climate conditions, they differ in  
265 soil hydrologic conditions and vegetation characteristics (section 2.1). The bulk density  
266 and porosity profiles were set to the values reported in Rydén et al. (1980), who  
267 suggested a decreasing trend of bulk density and an increasing trend of porosity from  
268 *palsa* ( $0.12 \text{ Mgm}^{-3}$  at surface; 92–93% within the upper 10 cm) to bog and fen ( $0.06$   
269  $\text{Mgm}^{-3}$  at surface; 96–97% within the upper 10 cm). The peatland soil carbon-to-nitrogen  
270 (C/N) ratios and pH values were assigned according to Hodgkins et al. (2014), who  
271 documented an increasing trend of pH from *palsa* (4.0), to bog (4.2), to fen (5.7), and a  
272 decreasing trend of soil organic matter C/N ratio from bog ( $46 \pm 18$ ), to *palsa* ( $39 \pm 24$ ), to  
273 fen ( $19 \pm 0.4$ ). Common values of field capacity (0.4) and wilting point (0.15) were used  
274 for the three peatland types (Deng et al., 2014).

275

### 276 **3 Results and Discussion**

#### 277 **3.1 GSWP3 climate comparison to observations**

278 As described in section 2.3, we extracted meteorological conditions at the  
279 Stordalen Mire from the GSWP3 climate reanalysis dataset. The closest GSWP3 grid cell  
280 was centered at  $68.0^\circ \text{N}$  and  $19.0^\circ \text{E}$ , which covers the Stordalen Mire and the ANS. The



281 annual mean air temperature and precipitation calculated at this GSWP3 grid cell were -  
282  $3.65\text{ }^{\circ}\text{C}$  and  $683.88\text{ mm y}^{-1}$ , respectively, for years 1913 to 2010. A cold bias ( $-3.09\text{ }^{\circ}\text{C}$ )  
283 was identified in the GSWP3 annual mean air temperature during the 1913 to 2010  
284 period, although a very high correlation coefficient ( $r = 0.99$ ) was found when compared  
285 with the ANS measurements (Figure 1a). Both time series exhibit an overall warming  
286 trend from the early 20<sup>th</sup> century to the present ( $0.01\text{ }^{\circ}\text{C y}^{-1}$ ), with an even more prominent  
287 warming trend from 1980 to 2010 ( $0.05\text{ }^{\circ}\text{C y}^{-1}$  [ANS] and  $0.04\text{ }^{\circ}\text{C y}^{-1}$  [GSWP3]).

288 Similarly, the GSWP3 annual total precipitation data correlates well with ANS  
289 measurements ( $r = 0.80$ ) but has a wet bias of  $380\text{ mm y}^{-1}$  between 1913 and 2010  
290 (Figure 1b). An increasing trend in annual total precipitation was recorded in both time  
291 series from the early 20<sup>th</sup> century to present ( $0.47\text{ mm y}^{-2}$  [ANS] and  $1.07\text{ mm y}^{-2}$   
292 [GSWP3]), although a decreasing trend was found from 1980 to 2010 ( $-0.56\text{ mm y}^{-2}$   
293 [ANS] and  $-2.39\text{ mm y}^{-2}$  [GSWP3]).

294 The seasonal cycle of the GSWP3 monthly mean air temperature also matches  
295 that measured at the ANS, with a very high correlation coefficient ( $r = 0.99$ ; Figure 2a).  
296 The underestimation bias and inter-annual variability of GSWP3 air temperature are  
297 greater in winter (maximum underestimate in December, at  $-4.52\text{ }^{\circ}\text{C}$ ) and smaller in  
298 summer (minimum underestimate in July, at  $-1.52\text{ }^{\circ}\text{C}$ ), respectively.

299 The magnitude and inter-annual variability of the GSWP3 monthly mean  
300 precipitation are comparable between winter and summer, while the ANS measurements  
301 exhibit stronger seasonality with lower magnitudes during winter. Despite the differences  
302 found in seasonal patterns, a high correlation coefficient ( $r = 0.64$ ) was found between the  
303 monthly mean precipitation extracted from GSWP3 and the ANS measurements. The



304 overestimation of monthly mean precipitation was greatest in December (43.25 mm  
305 month<sup>-1</sup>) and smallest in August (18.75 mm month<sup>-1</sup>).

306         These comparisons suggest that GSPW3 air temperature and precipitation data  
307 reasonably capture measured seasonal and long-term trends over past decades, but are  
308 biased cold and wet compared to observations, especially during winter. Similar cold and  
309 wet biases exist in CRUNCEP and ECMWF climate reanalysis datasets during our 2003  
310 to 2007 study period (Supplemental Material Figure 1). The calculated annual mean air  
311 temperature and precipitation at the Stordalen Mire for years 2003 to 2007 were -2.49 °C  
312 (precipitation 795.09 mm y<sup>-1</sup>), -2.46 °C (708.60 mm y<sup>-1</sup>), and -2.28 °C (765.67 mm y<sup>-1</sup>) in  
313 the GSWP3, CRUNCEP, and ECMWF climate reanalysis datasets, respectively.

314

## 315 **3.2 Model testing**

### 316 **3.2.1 Thaw depth**

317         We first evaluated *ecosys* against observations using bias-corrected climate  
318 forcing (i.e., the CTRL simulation). Predicted thaw depth agrees well with measurements  
319 collected from 2003 to 2007 for all examined peatland types (Figure 3), with a correlation  
320 coefficient of 0.95, 0.87, and 0.41 at the palsa, bog, and fen, respectively. Both  
321 simulations and observations show that the rate of thaw depth deepening in the summer  
322 varies with peatland type (i.e., relatively slow, moderate, and rapid at the palsa, bog, and  
323 fen sites, respectively).

324         Predicted and observed maximum thaw depth (i.e., Active Layer Depth, ALD) in  
325 the intact permafrost palsa was between 45 and 60 cm in September. In the partly thawed  
326 bog, the simulated thaw depth is slightly shallower than that observed before August. The



327 simulated bog thaw depth becomes greater than 90 cm by the end of August, which  
328 matches the time when measured thaw depth reaches its maximum. The thaw depth  
329 becomes greater than 90 cm by the end of July in the fully thawed fen. The patterns of  
330 thawing permafrost presented here are consistent with Deng et al. (2014), who simulated  
331 the same site using the DNDC model.

332

### 333 **3.2.2 CO<sub>2</sub> exchanges**

334 The daily Net Ecosystem Exchange (NEE) simulated in the CTRL simulation  
335 reasonably captures observed seasonal dynamics from 2003 to 2007 for all the examined  
336 peatland types (Figure 4). The simulations and observations showed net CO<sub>2</sub> uptake  
337 during summer and release during winter. The observations and simulations also showed  
338 large CO<sub>2</sub> emissions in the palsa site during Fall of 2004. Simulated Fall CO<sub>2</sub> bursts in the  
339 three sites in other years could not be confirmed because of a lack of observations during  
340 these periods. Similar to the patterns reported in Raz-Yaseef et al. (2016), some episodic  
341 CO<sub>2</sub> emission pulses were simulated as surface ice thaws in Spring, but there were no  
342 measurements to confirm those events. The correlation coefficients of the simulated and  
343 observed daily NEE ranged from 0.58 to 0.60, and most of the discrepancies between the  
344 simulations and observations were within the ranges of NEE variability measured at  
345 different subsites within the same peatland type.

346 As described in section 2.2, simulated CO<sub>2</sub> exchanges were evaluated for 3-hourly  
347 and daily time steps when quality-controlled measurements were available ( $R^2$  values and  
348 relative root mean squared errors (RRMSEs) shown in Table 2). Simulated NEE is in  
349 reasonable agreement with the 3-hourly NEE measurements with RRMSEs ranging



350 from 8.4 to 19.1%. Model performance was generally poorer at daily time steps, although  
351 the calculated RRMSEs were comparable to those reported in Deng et al. (2014). We  
352 suspect this degradation resulted from uncertainty in determining a daily NEE  
353 representative of the entire peatland type due to (1) limited daily data points (less than  
354 14% across the study period, Table 1) due to lack of continuous quality-controlled 3-  
355 hourly measurements and (2) the large variability of daily NEE ranges measured at  
356 different subsites within the same peatland type (Figure 4). Our results thus indicate that  
357 NEE is affected by thaw stage (Bäckstrand et al., 2010; Deng et al., 2014) and fine scale  
358 spatial heterogeneity of the system. More detailed measurements with higher spatial and  
359 temporal resolutions within the same peatland type would be necessary to characterize  
360 the effects of this type of heterogeneity.

361

### 362 **3.2.3 Water table depth and CH<sub>4</sub> exchanges**

363 Simulated water table depth generally captures observed seasonal patterns  
364 measured in the bog and fen sites from 2003 to 2007 (Figure 5a, c). During summer, the  
365 predicted bog water table depth fluctuates around the ground surface, and the predicted  
366 water table depth is at or above the ground surface in the fen. Water table depths  
367 simulated by *ecosys* are generally higher than the corresponding measurements in the  
368 bog, where measured water table depths are often below the ground surface with greater  
369 seasonal variability. Simulated fen water table depths have better overall fit to  
370 observations, being higher (~5 cm) than measurements in 2003 and 2004, close to  
371 measurements in 2005 and 2006, and slightly deeper (~2 cm) than measurements in 2007.  
372 The discrepancies in water table depth could be driven by the limitations of our one-



373 dimensional column simulation which inhibits lateral water transport and hinders the  
374 variations of water table depth, which is a particular issue in simulating the dynamic  
375 water table of the bog. A multi-dimensional simulation that includes realistic topographic  
376 effects could help improve the representation of water table dynamics, and estimates of  
377 the measurement uncertainty would help facilitate the assessment of simulation bias.

378 Simulated and measured daily CH<sub>4</sub> exchanges correlate reasonably well in the  
379 bog ( $r = 0.49$ ) and well in the fen ( $r = 0.65$ ) sites across the study period (Figure 5b, d).  
380 Both the simulations and observations have stronger CH<sub>4</sub> emissions during summer with  
381 peak emissions in late summer. Some episodic CH<sub>4</sub> emission pulses (Mastepanov et al.,  
382 2008) were simulated during shoulder seasons, and the simulated amount of post-growing  
383 season CH<sub>4</sub> emissions agrees well with those measured in 2007.

384 Most of the discrepancies between simulated and observed CH<sub>4</sub> emissions were  
385 within the variability of measurements across subsites within the same peatland type. The  
386 3-hourly and daily RRMSEs ranged from 11.1 to 22.3% (Table 2) and the daily RRMSEs  
387 were comparable to results presented in Deng et al. (2014). Our results show that model  
388 evaluation of CH<sub>4</sub> emissions with finer temporal resolution observations is not necessarily  
389 superior to evaluation with coarser temporal resolution. This result could be related to  
390 weaker CH<sub>4</sub> emission variability measured across subsites within the same peatland type  
391 (Figure 5b, d).

392

### 393 **3.3 Variability across the permafrost thaw gradient**

394 Thaw rate and ALD increase along the thaw gradient (i.e., palsa to bog to fen),  
395 and landscape variations are generally greater than simulated inter-annual variability



396 (Figure 6a). Maximum carbon uptake also increases along the thaw gradient, and  
397 variations across the landscape are comparable with simulated intra-seasonal and inter-  
398 annual variabilities (Figure 6b). The simulated mean seasonal cumulative NEE were  
399 calculated based on the seasonality identified in Bäckstrand et al. (2010), and the results  
400 show that the magnitude of mean growing season CO<sub>2</sub> uptake is highest in the fen and  
401 lowest in the palsa (Table 3). The same rank applies to the magnitude of mean CO<sub>2</sub>  
402 emissions over the non-growing season, although differences across the thaw gradient are  
403 smaller.

404 CH<sub>4</sub> emission rates increase significantly along the thaw gradient, and the palsa  
405 site emissions are negligible (Figure 6c). Mean cumulative CH<sub>4</sub> emissions simulated in  
406 the fen site are much higher than those in the bog site, and most CH<sub>4</sub> emissions occur  
407 during the growing season (Table 3). The higher CH<sub>4</sub> emissions in the fully thawed fen  
408 can be attributed to its faster thaw rate (Figure 6a) and a water table depth close to the  
409 surface (Figure 5c). Seasonal cumulative NEE and CH<sub>4</sub> emissions from observations  
410 could not be accessed due to the lack of continuous quality controlled carbon flux  
411 measurements during our study period (Table 1).

412

#### 413 **4. Climate sensitivity of permafrost thaw**

##### 414 **4.1 Thaw responses to climate**

415 For each of the four sets of simulations with different climate forcing (section  
416 2.5), simulated mean ALD from 2003 to 2007 is always greatest in the fen and lowest in  
417 the palsa (Figure 7). This consistent trend along the thaw gradient indicates that ALDs  
418 are largely regulated by their distinct ecological and hydrological conditions, because all



419 three sites had the same climate forcing in each set of simulations (i.e., CTRL, BIASED-  
420 COLD, BIASED-WET, and BIASED-COLD&BIASED-WET). Therefore, the intact  
421 permafrost palsa, partly thawed bog, and fully thawed fen have different resilience  
422 against the changes in climate forcing, and this type of ecosystem resilience plays an  
423 important role in determining ALD under changes in climate conditions.

424         Effects of climate on simulated ALD are similar across peatland types (Figure 7).  
425 With increased precipitation (BIASED-WET vs. CTRL), simulated ALD generally  
426 becomes deeper with greater inter-annual variability at all the examined peatland types.  
427 This effect is less prominent in the comparison between experiments BIASED-COLD  
428 and BIASED-COLD&BIASED-WET, possibly because the cold biases in these two  
429 experiments (section 3.1) constrain ALD variation. The simulated ALD also becomes  
430 deeper with higher air temperature (CTRL vs. BIASED-COLD; BIASED-WET vs.  
431 BIASED-COLD&BIASED-WET) at all the examined peatland types. This response is  
432 more evident in the comparison between experiments BIASED-WET and BIASED-  
433 COLD&BIASED-WET, probably driven by their wet bias (section 3.1) that facilitates  
434 ALD deepening (via increased thermal conductivity and advective heat transport; Grant  
435 et al. 2017a). Similar dependencies between ALD and climate were shown in Åkerman  
436 and Johansson (2008) and Johansson et al. (2013), based on multi-year measurements and  
437 snow manipulation experiments.

438         Therefore, the combined cold and wet biases in the GSWP3 climate reanalysis  
439 dataset could counteract their individual effects on simulated ALD development at the  
440 Stordalen Mire. Our results indicate a 28.6%, 0.7%, and 11.7% underestimation of ALD  
441 simulated in the palsa, bog, and fen sites, respectively, when applying the GSWP3



442 climate reanalysis data over this region without proper bias correction (BIASED-  
443 COLD&BIASED-WET vs. CTRL). Our sensitivity analysis suggests that projected  
444 warming and wetting trends (Collins et al., 2013) could significantly increase ALD in the  
445 Arctic, since increases in precipitation and air temperature can both contribute to ALD  
446 deepening.

447

#### 448 **4.2 Carbon budget responses to climate**

449 Annual mean (from 2003 to 2007) CO<sub>2</sub> and CH<sub>4</sub> exchanges simulated with the  
450 four climate forcing datasets (section 2.5) indicate a general CO<sub>2</sub> sink and CH<sub>4</sub> source,  
451 except the weak CO<sub>2</sub> emissions simulated at the fen in experiment BIASED-  
452 COLD&BIASED-WET (Figure 8a,b). Our results also indicate that differences in annual  
453 CO<sub>2</sub> and CH<sub>4</sub> exchanges across the four climate forcing datasets for a single peatland type  
454 are as large as those across peatland types for a single climate forcing dataset (Figure  
455 8a,b). These large CO<sub>2</sub> and CH<sub>4</sub> exchanges climate sensitivities demonstrate that the  
456 peatland's dynamical responses to climate have stronger effects on the carbon cycle than  
457 on ALDs (Figure 7).

458 With bias-corrected precipitation, increased air temperature (CTRL vs. BIASED-  
459 COLD) leads to stronger CO<sub>2</sub> uptake and greater CH<sub>4</sub> emissions at all the examined  
460 peatland types (Figure 8a,b), mainly because enhanced sedge growth facilitates carbon  
461 cycling under a warmer environment (results not shown). This air temperature sensitivity  
462 affects CO<sub>2</sub> and CH<sub>4</sub> exchanges within the same peatland type without significantly  
463 changing ALD (Figure 7). For both experiments, CO<sub>2</sub> uptake and CH<sub>4</sub> emissions are  
464 greatest in the fully thawed fen and lowest in the intact permafrost tundra, consistent with



465 the measurements reported in Bäckstrand et al. (2010) for the same period. Based on the  
466 Coupled Model Intercomparison Project, phase 5 (CMIP5) ESM simulations, arctic  
467 annual mean surface air temperature is projected to increase by  $8.5 \pm 2.1$  °C over the 21<sup>st</sup>  
468 century (Bintanja and Andry, 2017). This projected air temperature increase is more than  
469 double the air temperature difference between site-observed and GSWP3 temperatures,  
470 which could significantly enhance CH<sub>4</sub> emissions regardless of peat degradation into bog  
471 and fen.

472 On the other hand, wet biases (BIASED-WET and BIASED-COLD&BIASED-  
473 WET) increase CH<sub>4</sub> emissions in the peat site; wetter and colder conditions result in as  
474 much CH<sub>4</sub> release as the current fen sites, while wetter conditions alone drive peat  
475 emissions comparable to the current bog sites (Figure 8b). The large precipitation  
476 sensitivity found in peat CH<sub>4</sub> emissions could have strong effects on peat carbon  
477 cycling because arctic precipitation is projected to increase by 50 – 60 % towards the end  
478 of the twenty-first century (based on CMIP5 estimates; Bintanja and Andry, 2017). The  
479 comparison between experiments BIASED-WET and BIASED-COLD&BIASED-WET  
480 shows that in the peat, increased air temperature strengthens CO<sub>2</sub> uptake and weakens  
481 CH<sub>4</sub> emissions. This shift is primarily driven in the model by increased shrub and moss  
482 productivity under the warmer environment, which facilitate CO<sub>2</sub> uptake while drying out  
483 the soil and reducing CH<sub>4</sub> emissions (results not shown). In the bog and fen sites,  
484 increased air temperature under wet bias strengthens both the simulated CO<sub>2</sub> uptake and  
485 CH<sub>4</sub> emissions (BIASED-WET vs. BIASED-COLD&BIASED-WET), due to enhanced  
486 sedge growth under the warmer environment that facilitates carbon cycling in the  
487 experiment BIASED-WET.



488           We assessed the integrated effects of the changes in CO<sub>2</sub> and CH<sub>4</sub> exchanges  
489 identified in the full suite of simulations in terms of the Net Carbon Balance (NCB) and  
490 net emissions of greenhouse gases expressed as CO<sub>2</sub> equivalents (Net Greenhouse Gas  
491 Balance; NGGB). NCB was defined as the sum of the annual total CO<sub>2</sub> and CH<sub>4</sub>  
492 exchanges. NGGB was defined in a similar fashion as the NCB, but considers the greater  
493 radiative forcing potential of CH<sub>4</sub> than CO<sub>2</sub> (28 times over a 100-year horizon, Myhre et  
494 al., 2013) when calculating the annual total. The calculated NCB values are mostly  
495 negative because the stronger CO<sub>2</sub> uptake dominates the weaker CH<sub>4</sub> emissions (Figure  
496 8c). The results suggest that all the examined peatland types serve as net carbon sinks  
497 under current climate (CTRL), consistent with the estimates reported in Deng et al.  
498 (2014) and Lundin et al. (2016). We find a 24, 36, and 38 g C m<sup>-2</sup> y<sup>-1</sup> underestimation of  
499 NCB simulated in the palsa, bog, and fen sites, respectively, due to the cold and wet  
500 biases in the GSWP3 climate reanalysis dataset (BIASED-COLD&BIASED-WET vs.  
501 CTRL). NGGB is affected more strongly by CH<sub>4</sub> emissions (Figure 8d), due to its larger  
502 radiative forcing potential. NGGB values are positive over the bog and fen sites,  
503 suggesting that these sites can exhibit positive radiative forcing impacts despite being net  
504 carbon sinks. NGGB simulated in the palsa site is generally negative (i.e., a net sink from  
505 the atmosphere) due to lower CH<sub>4</sub> emissions, except for the simulation conducted without  
506 any climate bias correction (correcting only air temperature increased CH<sub>4</sub> emissions but  
507 not enough to compensate for the significantly higher CO<sub>2</sub> sink). Our results indicate that  
508 the simulated NGGB would be biased by 298, -66, and -252 g CO<sub>2</sub>-eq m<sup>-2</sup> y<sup>-1</sup> in the palsa,  
509 bog, and fen sites, respectively, without proper bias correction for the GSWP3 climate  
510 reanalysis dataset (BIASED-COLD&BIASED-WET vs. CTRL). Using the GSWP3



511 products directly thus effectively eliminates the positive radiative forcing from the  
512 expanding bog and fen sites, while creating a potentially dramatically inaccurate positive  
513 radiative forcing from the shrinking palsa sites.

514

### 515 **4.3 Climate sensitivity versus landscape heterogeneity**

516 Climate sensitivity and landscape heterogeneity are defined here as variability  
517 across the four climate forcing datasets for a single peatland type, and variability across  
518 three peatland types with bias-corrected climate (CTRL), respectively. We estimated  
519 carbon cycle variability associated with climate sensitivity and landscape heterogeneity to  
520 quantify the corresponding uncertainty in our annual carbon cycle assessments from 2003  
521 to 2007. Our results indicate that differences in simulated annual mean CO<sub>2</sub> exchanges  
522 and NCB from climate sensitivity are greater than those from landscape heterogeneity  
523 (Figure 8a,c); i.e., annual CO<sub>2</sub> uptake strength is more sensitive to climate forcing  
524 uncertainty than to peatland type representation. In terms of the simulated annual mean  
525 CH<sub>4</sub> emissions and NGGB, our results indicate that variability from climate sensitivity is  
526 comparable to those from landscape heterogeneity (Figure 8b,d). Therefore, bias-  
527 corrected climate and realistic peatland characterization are both necessary to reduce the  
528 uncertainty in representing CH<sub>4</sub> dynamics and its radiative forcing effects.

529 In addition to its effects on carbon cycle predictions, changes in climate  
530 conditions also affect permafrost degradation and thus induce changes in areal cover of  
531 peatland types. Malmer et al. (2005) showed that there were -0.95, 0.24, and 0.62 ha areal  
532 cover changes (-10.3%, 4.0%, and 46.3% percentage changes) from 1970 to 2000 in  
533 palsa, bog, and fen, respectively, at the Stordalen Mire. By applying the annual mean



534 CO<sub>2</sub> and CH<sub>4</sub> exchanges simulated with bias-corrected climate from 2003 to 2007, the  
535 areal cover changes from 1970 to 2000 alone would lead to -44 kg C y<sup>-1</sup>, 76 kg C y<sup>-1</sup>, and  
536 2076 kg CO<sub>2</sub>-eq y<sup>-1</sup> changes in annual mean CO<sub>2</sub> exchanges, CH<sub>4</sub> exchanges, and NGGB,  
537 respectively, at the Stordalen Mire. The changes in landscape scale carbon cycle  
538 dynamics indicate that the radiative warming impact of increased CH<sub>4</sub> emissions is large  
539 enough to offsets the radiative cooling impact of increased CO<sub>2</sub> uptake at the Stordalen  
540 Mire, consistent with the estimates reported in Deng et al. (2014). The areal cover  
541 changes across peatland types could persist or accelerate under the projected warming  
542 and wetting trends in the Arctic (Collins et al., 2013; Bintanja and Andry, 2017), which  
543 could stimulate CH<sub>4</sub> emissions and produce a stronger radiative warming impact.

544

## 545 **5. Conclusions**

546 We evaluated the climate bias in a widely used atmospheric reanalysis product  
547 (GSWP3) at our northern Sweden Stordalen Mire site. We then applied a comprehensive  
548 biogeochemistry model, *ecosys*, to estimate the effects of these biases on active layer  
549 development and carbon cycling across a thaw gradient at the site. Our results show that  
550 *ecosys* reasonably represented measured hydrological, thermal, and biogeochemical cycle  
551 processes in the intact permafrost palsa, partly thawed bog, and fully thawed fen. We  
552 found that the cold and wet biases in the GSWP3 climate reanalysis dataset significantly  
553 alter model simulations, leading to biases in simulated Active Layer Depths, Net Carbon  
554 Balance, and Net Greenhouse Gas Balance by up to 28.6%, 38 g C m<sup>-2</sup> y<sup>-1</sup>, and 298 g  
555 CO<sub>2</sub>-eq m<sup>-2</sup> y<sup>-1</sup>, respectively. The Net Carbon Balance simulated with bias-corrected  
556 climate suggests that all the examined peatland types are currently net carbon sinks from



557 the atmosphere, although the bog and fen sites can have positive radiative forcing impacts  
558 due to their higher CH<sub>4</sub> emissions.

559 Our results indicate that the annual means of ALD, CO<sub>2</sub> uptake, and CH<sub>4</sub>  
560 emissions generally increase along the permafrost thaw gradient at the Stordalen Mire  
561 under current climate, consistent with previous studies in this region. Our analysis  
562 suggests that palsa, bog, and fen landscape features differ strongly in their carbon cycling  
563 dynamics and have different responses to climate forcing biases. Differences in simulated  
564 CO<sub>2</sub> and CH<sub>4</sub> exchanges driven by uncertainty from climate forcing are as large as those  
565 from landscape heterogeneity across the examined permafrost thaw gradient. Model  
566 simulations demonstrate that the palsa site exhibits the strongest sensitivity to biases in  
567 air temperature and precipitation. The wet bias in GSWP3 could erroneously increase  
568 predicted CH<sub>4</sub> emissions from the palsa site to a magnitude comparable to emissions  
569 currently measured in bog and fen sites. These results also show that increased  
570 precipitation projected for high latitude regions could strongly accelerate CH<sub>4</sub> emissions  
571 from the palsa area, even without degradation of palsa into bog and fen. Future studies  
572 should thus recognize the effects of climate forcing uncertainty on carbon cycling, in  
573 addition to tracking changes in carbon budget associated with areal changes in permafrost  
574 degradation.

575

#### 576 **Acknowledgements**

577 This study was funded by the Genomic Science Program of the United States Department  
578 of Energy Office of Biological and Environmental Research under the ISOGENIE  
579 project, grant DE-SC0016440, to Lawrence Berkeley Laboratory under contract DE-



580 AC02-05CH11231, and by support from the Swedish Research Council (VR) to PMC.

581 We thank the Abisko Scientific Research Station of the Swedish Polar Research

582 Secretariat for providing the meteorological data.

583



584 **References**

585 Ahlström, A., Schurgers, G. and Smith, B.: The large influence of climate model bias on

586 terrestrial carbon cycle simulations, *Environmental Research Letters*, 12(1),

587 014004, doi:[10.1088/1748-9326/12/1/014004](https://doi.org/10.1088/1748-9326/12/1/014004), 2017.

588 Anav, A., Friedlingstein, P., Kidston, M., Bopp, L., Ciais, P., Cox, P., Jones, C., Jung,

589 M., Myneni, R. and Zhu, Z.: Evaluating the Land and Ocean Components of the

590 Global Carbon Cycle in the CMIP5 Earth System Models, *J. Climate*, 26(18),

591 6801–6843, doi:10.1175/JCLI-D-12-00417.1, 2013.

592 Arneeth, A., Sitch, S., Pongratz, J., Stocker, B. D., Ciais, P., Poulter, B., Bayer, A. D.,

593 Bondeau, A., Calle, L., Chini, L. P., Gasser, T., Fader, M., Friedlingstein, P.,

594 Kato, E., Li, W., Lindeskog, M., Nabel, J. E. M. S., Pugh, T. A. M., Robertson,

595 E., Viovy, N., Yue, C. and Zaehle, S.: Historical carbon dioxide emissions caused

596 by land-use changes are possibly larger than assumed, *Nature Geoscience*, 10(2),

597 79–84, doi:[10.1038/ngeo2882](https://doi.org/10.1038/ngeo2882), 2017.

598 Bäckstrand, K., Crill, P. M., Mastepanov, M., Christensen, T. R. and Bastviken, D.: Non-

599 methane volatile organic compound flux from a subarctic mire in Northern

600 Sweden, *Tellus B*, 60(2), 226–237, doi:[10.1111/j.1600-0889.2007.00331.x](https://doi.org/10.1111/j.1600-0889.2007.00331.x),

601 2008a.

602 Bäckstrand, K., Crill, P. M., Mastepanov, M., Christensen, T. R. and Bastviken, D.: Total

603 hydrocarbon flux dynamics at a subarctic mire in northern Sweden, *Journal of*

604 *Geophysical Research: Biogeosciences*, 113(G3), doi:[10.1029/2008JG000703](https://doi.org/10.1029/2008JG000703),

605 2008b.



- 606 Backstrand, K., Crill, P. M., ski, M. J.-K., Mastepanov, M., Christensen, T. R. and  
607 Bastviken, D.: Annual carbon gas budget for a subarctic peatland, Northern  
608 Sweden, 14, 2010.
- 609 Berrisford, P., Dee, D. P., Poli, P., Brugge, R., Fielding, K., Fuentes, M., Kållberg, P. W.,  
610 Kobayashi, S., Uppala, S. and Simmons, A.: The ERA-Interim archive Version  
611 2.0, 2011.
- 612 Bintanja, R. and Andry, O.: Towards a rain-dominated Arctic, Nature Climate Change,  
613 7(4), 263–267, doi:[10.1038/nclimate3240](https://doi.org/10.1038/nclimate3240), 2017.
- 614 Callaghan, T. V., Bergholm, F., Christensen, T. R., Jonasson, C., Kokfelt, U. and  
615 Johansson, M.: A new climate era in the sub-Arctic: Accelerating climate changes  
616 and multiple impacts, Geophysical Research Letters, 37(14),  
617 doi:[10.1029/2009GL042064](https://doi.org/10.1029/2009GL042064), 2010.
- 618 Chang, K.-Y., Paw U, K. T. and Chen, S.-H.: The importance of carbon-nitrogen  
619 biogeochemistry on water vapor and carbon fluxes as elucidated by a multiple  
620 canopy layer higher order closure land surface model, Agricultural and Forest  
621 Meteorology, 259, 60–74, doi:[10.1016/j.agrformet.2018.04.009](https://doi.org/10.1016/j.agrformet.2018.04.009), 2018.
- 622 Christensen, T. R., Johansson, T., Åkerman, H. J., Mastepanov, M., Malmer, N., Friborg,  
623 T., Crill, P. and Svensson, B. H.: Thawing sub-arctic permafrost: Effects on  
624 vegetation and methane emissions, Geophysical Research Letters, 31(4),  
625 doi:[10.1029/2003GL018680](https://doi.org/10.1029/2003GL018680), 2004.
- 626 Collins, M., R. Knutti, J. Arblaster, J.-L. Dufresne, T. Fichefet, P. Friedlingstein, X. Gao,  
627 W.J. Gutowski, T. Johns, G. Krinner, M. Shongwe, C. Tebaldi, A.J. Weaver and  
628 M. Wehner, 2013: Long-term Climate Change: Projections, Commitments and



- 629 Irreversibility. Climate Change 2013: The Physical Science Basis. Contribution of  
630 Working Group I to the Fifth Assessment Report of the Intergovernmental Panel  
631 on Climate Change. T. F. Stocker et al., Eds., Cambridge University Press, 1029-  
632 1136.
- 633 Compo, G. P., Whitaker, J. S., Sardeshmukh, P. D., Matsui, N., Allan, R. J., Yin, X.,  
634 Gleason, B. E., Vose, R. S., Rutledge, G., Bessemoulin, P., Brönnimann, S.,  
635 Brunet, M., Crouthamel, R. I., Grant, A. N., Groisman, P. Y., Jones, P. D., Kruk,  
636 M. C., Kruger, A. C., Marshall, G. J., Maugeri, M., Mok, H. Y., Nordli, Ø., Ross,  
637 T. F., Trigo, R. M., Wang, X. L., Woodruff, S. D. and Worley, S. J.: The  
638 Twentieth Century Reanalysis Project, Quarterly Journal of the Royal  
639 Meteorological Society, 137(654), 1–28, doi:[10.1002/qj.776](https://doi.org/10.1002/qj.776), 2011.
- 640 Cooper, M. D. A., Estop-Aragonés, C., Fisher, J. P., Thierry, A., Garnett, M. H.,  
641 Charman, D. J., Murton, J. B., Phoenix, G. K., Treharne, R., Kokelj, S. V., Wolfe,  
642 S. A., Lewkowicz, A. G., Williams, M. and Hartley, I. P.: Limited contribution of  
643 permafrost carbon to methane release from thawing peatlands, Nature Climate  
644 Change, 7(7), 507–511, doi:[10.1038/nclimate3328](https://doi.org/10.1038/nclimate3328), 2017.
- 645 Cox, P. M., Betts, R. A., Jones, C. D., Spall, S. A. and Totterdell, I. J.: Acceleration of  
646 global warming due to carbon-cycle feedbacks in a coupled climate model, 408,  
647 4, 2000.
- 648 Deng, J., Li, C., Frohking, S., Zhang, Y., Bäckstrand, K. and Crill, P.: Assessing effects of  
649 permafrost thaw on C fluxes based on multiyear modeling across a permafrost  
650 thaw gradient at Stordalen, Sweden, Biogeosciences, 11(17), 4753–4770,  
651 doi:[10.5194/bg-11-4753-2014](https://doi.org/10.5194/bg-11-4753-2014), 2014.



- 652 Dimitrov, D. D., Bhatti, J. S. and Grant, R. F.: The transition zones (ecotone) between  
653 boreal forests and peatlands: Ecological controls on ecosystem productivity along  
654 a transition zone between upland black spruce forest and a poor forested fen in  
655 central Saskatchewan, *Ecological Modelling*, 291, 96–108,  
656 doi:10.1016/j.ecolmodel.2014.07.020, 2014.
- 657 Dimitrov Dimitre D., Grant Robert F., Lafleur Peter M. and Humphreys Elyn R.:  
658 Modeling the effects of hydrology on gross primary productivity and net  
659 ecosystem productivity at Mer Bleue bog, *Journal of Geophysical Research:*  
660 *Biogeosciences*, 116(G4), doi:10.1029/2010JG001586, 2011.
- 661 Dirmeyer, P. A.: A History and Review of the Global Soil Wetness Project (GSWP),  
662 *Journal of Hydrometeorology*, 12(5), 729–749, doi:[10.1175/JHM-D-10-05010.1](https://doi.org/10.1175/JHM-D-10-05010.1),  
663 2011.
- 664 Friedlingstein, P., Cox, P., Betts, R., Bopp, L., von Bloh, W., Brovkin, V., Cadule, P.,  
665 Doney, S., Eby, M., Fung, I., Bala, G., John, J., Jones, C., Joos, F., Kato, T.,  
666 Kawamiya, M., Knorr, W., Lindsay, K., Matthews, H. D., Raddatz, T., Rayner, P.,  
667 Reick, C., Roeckner, E., Schnitzler, K.-G., Schnur, R., Strassmann, K., Weaver,  
668 A. J., Yoshikawa, C. and Zeng, N.: Climate–Carbon Cycle Feedback Analysis:  
669 Results from the C<sup>4</sup> MIP Model Intercomparison, *Journal of Climate*, 19(14),  
670 3337–3353, doi:[10.1175/JCLI3800.1](https://doi.org/10.1175/JCLI3800.1), 2006.
- 671 Friedlingstein, P., Meinshausen, M., Arora, V. K., Jones, C. D., Anav, A., Liddicoat, S.  
672 K. and Knutti, R.: Uncertainties in CMIP5 Climate Projections due to Carbon  
673 Cycle Feedbacks, *Journal of Climate*, 27(2), 511–526, doi:[10.1175/JCLI-D-12-](https://doi.org/10.1175/JCLI-D-12-00579.1)  
674 [00579.1](https://doi.org/10.1175/JCLI-D-12-00579.1), 2014.



- 675 Ghimire, B., Riley, W. J., Koven, C. D., Mu, M. and Randerson, J. T.: Representing leaf  
676 and root physiological traits in CLM improves global carbon and nitrogen cycling  
677 predictions, *Journal of Advances in Modeling Earth Systems*, 8(2), 598–613,  
678 doi:[10.1002/2015MS000538](https://doi.org/10.1002/2015MS000538), 2016.
- 679 Grant, R. F.: Modelling changes in nitrogen cycling to sustain increases in forest  
680 productivity under elevated atmospheric CO<sub>2</sub> and contrasting site conditions,  
681 *Biogeosciences*, 10(11), 7703–7721, doi:10.5194/bg-10-7703-2013, 2013.
- 682 Grant, R. F.: Nitrogen mineralization drives the response of forest productivity to soil  
683 warming: Modelling in ecosys vs. measurements from the Harvard soil heating  
684 experiment, *Ecological Modelling*, 288, 38–46,  
685 doi:10.1016/j.ecolmodel.2014.05.015, 2014.
- 686 Grant R. F. and Flanagan L. B.: Modeling stomatal and nonstomatal effects of water  
687 deficits on CO<sub>2</sub> fixation in a semiarid grassland, *Journal of Geophysical*  
688 *Research: Biogeosciences*, 112(G3), doi:10.1029/2006JG000302, 2007.
- 689 Grant, R. F. and Roulet, N. T.: Methane efflux from boreal wetlands: Theory and testing  
690 of the ecosystem model Ecosys with chamber and tower flux measurements,  
691 *Global Biogeochemical Cycles*, 16(4), 2-1-2–16, doi:10.1029/2001GB001702,  
692 2002.
- 693 Grant, R. F., Oechel, W. C. and Ping, C.-L.: Modelling carbon balances of coastal arctic  
694 tundra under changing climate, *Global Change Biology*, 9(1), 16–36,  
695 doi:10.1046/j.1365-2486.2003.00549.x, 2003.
- 696 Grant, R. F., Black, T. A., Humphreys, E. R. and Morgenstern, K.: Changes in net  
697 ecosystem productivity with forest age following clearcutting of a coastal



- 698 Douglas-fir forest: testing a mathematical model with eddy covariance  
699 measurements along a forest chronosequence, *Tree Physiol.*, 27(1), 115–131,  
700 2007a.
- 701 Grant, R. F., Arkebauer, T. J., Dobermann, A., Hubbard, K. G., Schimelfenig, T. T.,  
702 Suyker, A. E., Verma, S. B. and Walters, D. T.: Net Biome Productivity of  
703 Irrigated and Rainfed Maize–Soybean Rotations: Modeling vs. Measurements,  
704 *Agronomy Journal*, 99(6), 1404, doi:10.2134/agronj2006.0308, 2007b.
- 705 Grant, R. F., Barr, A. G., Black, T. A., Gaumont-Guay, D., Iwashita, H., Kidson, J.,  
706 McCAUGHEY, H., Morgenstern, K., Murayama, S., Nestic, Z., Saigusa, N.,  
707 Shashkov, A. and Zha, T.: Net ecosystem productivity of boreal jack pine stands  
708 regenerating from clearcutting under current and future climates, *Global Change*  
709 *Biology*, 13(7), 1423–1440, doi:10.1111/j.1365-2486.2007.01363.x, 2007c.
- 710 Grant, R. F., Margolis, H. A., Barr, A. G., Black, T. A., Dunn, A. L., Bernier, P. Y. and  
711 Bergeron, O.: Changes in net ecosystem productivity of boreal black spruce  
712 stands in response to changes in temperature at diurnal and seasonal time scales,  
713 *Tree Physiology*, 29(1), 1–17, doi:10.1093/treephys/tpn004, 2009a.
- 714 Grant, R. F., Barr, A. G., Black, T. A., Margolis, H. A., Dunn, A. L., Metsaranta, J.,  
715 Wang, S., McCaughey, J. H. and Bourque, C. A.: Interannual variation in net  
716 ecosystem productivity of Canadian forests as affected by regional weather  
717 patterns – A Fluxnet-Canada synthesis, *Agricultural and Forest Meteorology*,  
718 149(11), 2022–2039, doi:10.1016/j.agrformet.2009.07.010, 2009b.
- 719 Grant, R. F., Hutyyra, L. R., Oliveira, R. C., Munger, J. W., Saleska, S. R. and Wofsy, S.  
720 C.: Modeling the carbon balance of Amazonian rain forests: resolving ecological



- 721 controls on net ecosystem productivity, *Ecological Monographs*, 79(3), 445–463,  
722 doi:10.1890/08-0074.1, 2009c.
- 723 Grant, R. F., Barr, A. G., Black, T. A., Margolis, H. A., Mccaughey, J. H. and Trofymow,  
724 J. A.: Net ecosystem productivity of temperate and boreal forests after  
725 clearcutting—a Fluxnet-Canada measurement and modelling synthesis, *Tellus B:  
726 Chemical and Physical Meteorology*, 62(5), 475–496, doi:10.1111/j.1600-  
727 0889.2010.00500.x, 2010.
- 728 Grant, R. F., Kimball, B. A., Conley, M. M., White, J. W., Wall, G. W. and Ottman, M.  
729 J.: Controlled Warming Effects on Wheat Growth and Yield: Field Measurements  
730 and Modeling, *Agronomy Journal*, 103(6), 1742–1754,  
731 doi:10.2134/agronj2011.0158, 2011a.
- 732 Grant, R. F., Humphreys, E. R., Lafleur, P. M. and Dimitrov, D. D.: Ecological controls  
733 on net ecosystem productivity of a mesic arctic tundra under current and future  
734 climates, *Journal of Geophysical Research: Biogeosciences*, 116(G1),  
735 doi:10.1029/2010JG001555, 2011b.
- 736 Grant, R. F., Baldocchi, D. D. and Ma, S.: Ecological controls on net ecosystem  
737 productivity of a seasonally dry annual grassland under current and future  
738 climates: Modelling with ecosys, *Agricultural and Forest Meteorology*, 152, 189–  
739 200, doi:10.1016/j.agrformet.2011.09.012, 2012a.
- 740 Grant, R. F., Desai, A. R. and Sulman, B. N.: Modelling contrasting responses of wetland  
741 productivity to changes in water table depth, *Biogeosciences*, 9(11), 4215–4231,  
742 doi:10.5194/bg-9-4215-2012, 2012b.



- 743 Grant R. F., Humphreys E. R. and Lafleur P. M.: Ecosystem CO<sub>2</sub> and CH<sub>4</sub> exchange in a  
744 mixed tundra and a fen within a hydrologically diverse Arctic landscape: 1.  
745 Modeling versus measurements, *Journal of Geophysical Research:*  
746 *Biogeosciences*, 120(7), 1366–1387, doi:[10.1002/2014JG002888](https://doi.org/10.1002/2014JG002888), 2015.
- 747 Grant, R. F., Mekonnen, Z. A., Riley, W. J., Wainwright, H. M., Graham, D. and Torn,  
748 M. S.: Mathematical Modelling of Arctic Polygonal Tundra with *Ecosys*: 1.  
749 Microtopography Determines How Active Layer Depths Respond to Changes in  
750 Temperature and Precipitation, *Journal of Geophysical Research: Biogeosciences*,  
751 122(12), 3161–3173, doi:[10.1002/2017JG004035](https://doi.org/10.1002/2017JG004035), 2017a.
- 752 Grant, R. F., Mekonnen, Z. A., Riley, W. J., Arora, B. and Torn, M. S.: Mathematical  
753 Modelling of Arctic Polygonal Tundra with *Ecosys*: 2. Microtopography  
754 Determines How CO<sub>2</sub> and CH<sub>4</sub> Exchange Responds to Changes in Temperature  
755 and Precipitation: GHG Exchange in Arctic Polygonal Tundra, *Journal of*  
756 *Geophysical Research: Biogeosciences*, 122(12), 3174–3187,  
757 doi:[10.1002/2017JG004037](https://doi.org/10.1002/2017JG004037), 2017b.
- 758 Guo, D., Wang, H. and Wang, A.: Sensitivity of Historical Simulation of the Permafrost  
759 to Different Atmospheric Forcing Data Sets from 1979 to 2009, *Journal of*  
760 *Geophysical Research: Atmospheres*, 122(22), 12,269–12,284,  
761 doi:[10.1002/2017JD027477](https://doi.org/10.1002/2017JD027477), 2017.
- 762 Harris, I., Jones, P. D., Osborn, T. J. and Lister, D. H.: Updated high-resolution grids of  
763 monthly climatic observations – the CRU TS3.10 Dataset, *International Journal of*  
764 *Climatology*, 34(3), 623–642, doi:[10.1002/joc.3711](https://doi.org/10.1002/joc.3711), n.d.



- 765 Hodgkins, S. B., Tfaily, M. M., McCalley, C. K., Logan, T. A., Crill, P. M., Saleska, S.  
766 R., Rich, V. I. and Chanton, J. P.: Changes in peat chemistry associated with  
767 permafrost thaw increase greenhouse gas production, Proceedings of the National  
768 Academy of Sciences, 111(16), 5819–5824, doi:[10.1073/pnas.1314641111](https://doi.org/10.1073/pnas.1314641111), 2014.
- 769 van den Hurk, B., Kim, H., Krinner, G., Seneviratne, S. I., Derksen, C., Oki, T., Douville,  
770 H., Colin, J., Ducharne, A., Cheruy, F., Viovy, N., Puma, M. J., Wada, Y., Li, W.,  
771 Jia, B., Alessandri, A., Lawrence, D. M., Weedon, G. P., Ellis, R., Hagemann, S.,  
772 Mao, J., Flanner, M. G., Zampieri, M., Materia, S., Law, R. M. and Sheffield, J.:  
773 LS3MIP (v1.0) contribution to CMIP6: the Land Surface, Snow and Soil moisture  
774 Model Intercomparison Project – aims, setup and expected outcome,  
775 Geoscientific Model Development, 9(8), 2809–2832, doi:[10.5194/gmd-9-2809-](https://doi.org/10.5194/gmd-9-2809-2016)  
776 2016, 2016.
- 777 Hugelius, G., Strauss, J., Zubrzycki, S., Harden, J. W., Schuur, E. A. G., Ping, C.-L.,  
778 Schirrmeister, L., Grosse, G., Michaelson, G. J., Koven, C. D.,  
779 O&apos;Donnell, J. A., Elberling, B., Mishra, U., Camill, P., Yu, Z.,  
780 Palmtag, J. and Kuhry, P.: Estimated stocks of circumpolar permafrost carbon  
781 with quantified uncertainty ranges and identified data gaps, Biogeosciences,  
782 11(23), 6573–6593, doi:[10.5194/bg-11-6573-2014](https://doi.org/10.5194/bg-11-6573-2014), 2014.
- 783 IPCC, 2014: Climate Change 2014: Synthesis Report. Contribution of Working Groups I,  
784 II and III to the Fifth Assessment Report of the Intergovernmental Panel on  
785 Climate Change [Core Writing Team, R.K. Pachauri and L.A. Meyer (eds.)].  
786 IPCC, Geneva, Switzerland, 151 pp.



- 787 Johansson, M., Callaghan, T. V., Bosiö, J., Åkerman, H. J., Jackowicz-Korczynski, M.  
788 and Christensen, T. R.: Rapid responses of permafrost and vegetation to  
789 experimentally increased snow cover in sub-arctic Sweden, *Environmental*  
790 *Research Letters*, 8(3), 035025, doi:[10.1088/1748-9326/8/3/035025](https://doi.org/10.1088/1748-9326/8/3/035025), 2013.
- 791 Johansson, T., Malmer, N., Crill, P. M., Friborg, T., Åkerman, J. H., Mastepanov, M. and  
792 Christensen, T. R.: Decadal vegetation changes in a northern peatland, greenhouse  
793 gas fluxes and net radiative forcing, *Global Change Biology*, 12(12), 2352–2369,  
794 doi:[10.1111/j.1365-2486.2006.01267.x](https://doi.org/10.1111/j.1365-2486.2006.01267.x), 2006.
- 795 Kalnay, E., Kanamitsu, M., Kistler, R., Collins, W., Deaven, D., Gandin, L., Iredell, M.,  
796 Saha, S., White, G., Woollen, J., Zhu, Y., Chelliah, M., Ebisuzaki, W., Higgins,  
797 W., Janowiak, J., Mo, K. C., Ropelewski, C., Wang, J., Leetmaa, A., Reynolds,  
798 R., Jenne, R. and Joseph, D.: The NCEP/NCAR 40-Year Reanalysis Project, *Bull.*  
799 *Amer. Meteor. Soc.*, 77(3), 437–472, doi:10.1175/1520-  
800 0477(1996)077<0437:TNYRP>2.0.CO;2, 1996.
- 801 Kanamitsu, M., Ebisuzaki, W., Woollen, J., Yang, S.-K., Hnilo, J. J., Fiorino, M. and  
802 Potter, G. L.: NCEP–DOE AMIP-II Reanalysis (R-2), *Bull. Amer. Meteor. Soc.*,  
803 83(11), 1631–1644, doi:10.1175/BAMS-83-11-1631, 2002.
- 804 Lundin, E. J., Klaminder, J., Giesler, R., Persson, A., Olefeldt, D., Heliasz, M.,  
805 Christensen, T. R. and Karlsson, J.: Is the subarctic landscape still a carbon sink?  
806 Evidence from a detailed catchment balance, *Geophysical Research Letters*,  
807 43(5), 1988–1995, doi:[10.1002/2015GL066970](https://doi.org/10.1002/2015GL066970), 2016.
- 808 Malmer, N., Johansson, T., Olsrud, M. and Christensen, T. R.: Vegetation, climatic  
809 changes and net carbon sequestration in a North-Scandinavian subarctic mire over



- 810 30 years, *Global Change Biology*, 11(11), 1895–1909, doi:[10.1111/j.1365-](https://doi.org/10.1111/j.1365-2486.2005.01042.x)  
811 [2486.2005.01042.x](https://doi.org/10.1111/j.1365-2486.2005.01042.x), 2005.
- 812 Mastepanov, M., Sigsgaard, C., Dlugokencky, E. J., Houweling, S., Ström, L., Tamstorf,  
813 M. P. and Christensen, T. R.: Large tundra methane burst during onset of  
814 freezing, *Nature*, 456(7222), 628–630, doi:[10.1038/nature07464](https://doi.org/10.1038/nature07464), 2008.
- 815 McCalley, C. K., Woodcroft, B. J., Hodgkins, S. B., Wehr, R. A., Kim, E.-H., Mondav,  
816 R., Crill, P. M., Chanton, J. P., Rich, V. I., Tyson, G. W. and Saleska, S. R.:  
817 Methane dynamics regulated by microbial community response to permafrost  
818 thaw, *Nature*, 514(7523), 478–481, doi:[10.1038/nature13798](https://doi.org/10.1038/nature13798), 2014.
- 819 Mezbahuddin, M., Grant, R. F. and Hirano, T.: Modelling effects of seasonal variation in  
820 water table depth on net ecosystem CO<sub>2</sub> exchange of a tropical peatland,  
821 *Biogeosciences*, 11(3), 577–599, doi:[10.5194/bg-11-577-2014](https://doi.org/10.5194/bg-11-577-2014), 2014.
- 822 Mondav, R., McCalley, C. K., Hodgkins, S. B., Frolking, S., Saleska, S. R., Rich, V. I.,  
823 Chanton, J. P. and Crill, P. M.: Microbial network, phylogenetic diversity and  
824 community membership in the active layer across a permafrost thaw gradient,  
825 *Environmental Microbiology*, 19(8), 3201–3218, doi:[10.1111/1462-2920.13809](https://doi.org/10.1111/1462-2920.13809),  
826 2017.
- 827 Mondav, R., Woodcroft, B. J., Kim, E.-H., McCalley, C. K., Hodgkins, S. B., Crill, P.  
828 M., Chanton, J., Hurst, G. B., VerBerkmoes, N. C., Saleska, S. R., Hugenholtz, P.,  
829 Rich, V. I. and Tyson, G. W.: Discovery of a novel methanogen prevalent in  
830 thawing permafrost, *Nature Communications*, 5, 3212, doi:[10.1038/ncomms4212](https://doi.org/10.1038/ncomms4212),  
831 2014.



- 832 Myhre, G., D. Shindell, F.-M. Bréon, W. Collins, J. Fuglestedt, J. Huang, D. Koch, J.-F.  
833 Lamarque, D. Lee, B. Mendoza, T. Nakajima, A. Robock, G. Stephens, T.  
834 Takemura and H. Zhang, 2013: Anthropogenic and Natural Radiative Forcing. In:  
835 Climate Change 2013: The Physical Science Basis. Contribution of Working  
836 Group I to the Fifth Assessment Report of the Intergovernmental Panel on  
837 Climate Change [Stocker, T.F., D. Qin, G.-K. Plattner, M. Tignor, S.K. Allen, J.  
838 Boschung, A. Nauels, Y. Xia, V. Bex and P.M. Midgley (eds.)]. Cambridge  
839 University Press, Cambridge, United Kingdom and New York, NY, USA, pp.  
840 659–740, doi:10.1017/CBO9781107415324.018.
- 841 Olefeldt, D. and Roulet, N. T.: Effects of permafrost and hydrology on the composition  
842 and transport of dissolved organic carbon in a subarctic peatland complex, Journal  
843 of Geophysical Research: Biogeosciences, 117(G1), doi:[10.1029/2011JG001819](https://doi.org/10.1029/2011JG001819),  
844 2012.
- 845 Piao, S., Liu, Z., Wang, T., Peng, S., Ciais, P., Huang, M., Ahlstrom, A., Burkhardt, J. F.,  
846 Chevallier, F., Janssens, I. A., Jeong, S.-J., Lin, X., Mao, J., Miller, J.,  
847 Mohammat, A., Myneni, R. B., Peñuelas, J., Shi, X., Stohl, A., Yao, Y., Zhu, Z.  
848 and Tans, P. P.: Weakening temperature control on the interannual variations of  
849 spring carbon uptake across northern lands, Nature Climate Change, 7(5), 359–  
850 363, doi:[10.1038/nclimate3277](https://doi.org/10.1038/nclimate3277), 2017.
- 851 Raz-Yaseef, N., Torn, M. S., Wu, Y., Billesbach, D. P., Liljedahl, A. K., Kneafsey, T. J.,  
852 Romanovsky, V. E., Cook, D. R. and Wullschleger, S. D.: Large CO<sub>2</sub> and CH<sub>4</sub>  
853 emissions from polygonal tundra during spring thaw in northern Alaska,



- 854 Geophysical Research Letters, 44(1), 504–513, doi:[10.1002/2016GL071220](https://doi.org/10.1002/2016GL071220),  
855 2017.
- 856 Rydén, B. E., Fors, L. and Kostov, L.: Physical Properties of the Tundra Soil-Water  
857 System at Stordalen, Abisko, Ecological Bulletins, (30), 27–54, 1980.
- 858 Schuur, E. a. G., McGuire, A. D., Schädel, C., Grosse, G., Harden, J. W., Hayes, D. J.,  
859 Hugelius, G., Koven, C. D., Kuhry, P., Lawrence, D. M., Natali, S. M., Olefeldt,  
860 D., Romanovsky, V. E., Schaefer, K., Turetsky, M. R., Treat, C. C. and Vonk, J.  
861 E.: Climate change and the permafrost carbon feedback, Nature, 520(7546), 171–  
862 179, doi:10.1038/nature14338, 2015.
- 863 Tokida, T., Miyazaki, T., Mizoguchi, M., Nagata, O., Takakai, F., Kagemoto, A. and  
864 Hatano, R.: Falling atmospheric pressure as a trigger for methane ebullition from  
865 peatland, Global Biogeochemical Cycles, 21(2), doi:10.1029/2006GB002790,  
866 2007.
- 867 Viovy, N.: CRUNCEP Version 7 - Atmospheric Forcing Data for the Community Land  
868 Model, Research Data Archive at the National Center for Atmospheric Research,  
869 Computational and Information Systems Laboratory, Boulder CO.
- 870 Wickland, K. P., Striegl, R. G., Neff, J. C. and Sachs, T.: Effects of permafrost melting  
871 on CO<sub>2</sub> and CH<sub>4</sub> exchange of a poorly drained black spruce lowland, Journal of  
872 Geophysical Research: Biogeosciences, 111(G2), doi:[10.1029/2005JG000099](https://doi.org/10.1029/2005JG000099),  
873 2006.
- 874 Woodcroft, B. J., Singleton, C. M., Boyd, J. A., Evans, P. N., Emerson, J. B., Zayed, A.  
875 A. F., Hoelzle, R. D., Lamberton, T. O., McCalley, C. K., Hodgkins, S. B.,  
876 Wilson, R. M., Purvine, S. O., Nicora, C. D., Li, C., Frohking, S., Chanton, J. P.,



- 877 Crill, P. M., Saleska, S. R., Rich, V. I. and Tyson, G. W.: Genome-centric view of  
878 carbon processing in thawing permafrost, *Nature*, doi:[10.1038/s41586-018-0338-](https://doi.org/10.1038/s41586-018-0338-1)  
879 [1](https://doi.org/10.1038/s41586-018-0338-1), 2018.
- 880 Wu, Z., Ahlström, A., Smith, B., Ardö, J., Eklundh, L., Fensholt, R. and Lehsten, V.:  
881 Climate data induced uncertainty in model-based estimations of terrestrial  
882 primary productivity, *Environmental Research Letters*, 12(6), 064013,  
883 doi:[10.1088/1748-9326/aa6fd8](https://doi.org/10.1088/1748-9326/aa6fd8), 2017.
- 884 Yoshimura, K. and Kanamitsu, M.: Dynamical Global Downscaling of Global  
885 Reanalysis, *Monthly Weather Review*, 136(8), 2983–2998,  
886 doi:[10.1175/2008MWR2281.1](https://doi.org/10.1175/2008MWR2281.1), 2008.
- 887 Zaehle, S., Friend, A. D., Friedlingstein, P., Dentener, F., Peylin, P. and Schulz, M.:  
888 Carbon and nitrogen cycle dynamics in the O-CN land surface model: 2. Role of  
889 the nitrogen cycle in the historical terrestrial carbon balance, *Global*  
890 *Biogeochemical Cycles*, 24(1), doi:[10.1029/2009GB003522](https://doi.org/10.1029/2009GB003522), 2010.
- 891 Zimov, S. A., Davydov, S. P., Zimova, G. M., Davydova, A. I., Schuur, E. a. G., Dutta,  
892 K. and Chapin, F. S.: Permafrost carbon: Stock and decomposability of a globally  
893 significant carbon pool, *Geophysical Research Letters*, 33(20),  
894 doi:[10.1029/2006GL027484](https://doi.org/10.1029/2006GL027484), 2006.
- 895



896 Table 1. Temporal coverage of quality-controlled CO<sub>2</sub> and CH<sub>4</sub> exchanges measured by  
 897 automatic chambers at the three peatland types in the Stordalen Mire during the years  
 898 2002 to 2007.

Sites	Number of data points	CO <sub>2</sub>		Number of data points	CH <sub>4</sub>	
		3 Hourly coverage (%)	Daily coverage (%)		3 Hourly coverage (%)	Daily coverage (%)
Palsa	12752	65.8	12.4	N/A	N/A	N/A
Bog	12821	68.5	12.7	6660	96.2	25.0
Fen	8989	63.8	13.7	4923	90.5	33.7

899



900 Table 2. The evaluation of the 3 hourly and daily CO<sub>2</sub> and CH<sub>4</sub> exchanges simulated at  
 901 the palsa, bog, and fen sites. RRMSEs are relative root mean squared errors.

Sites	C component	3-Hourly		Daily	
		R <sup>2</sup>	RRMSEs (%)	R <sup>2</sup>	RRMSEs (%)
Palsa	CO <sub>2</sub>	0.48	13.4	0.36	18.3
Bog	CO <sub>2</sub>	0.63	19.1	0.44	35.8
	CH <sub>4</sub>	0.31	16.3	0.47	22.3
Fen	CO <sub>2</sub>	0.64	8.4	0.43	25.5
	CH <sub>4</sub>	0.44	11.1	0.54	16.9

902

903

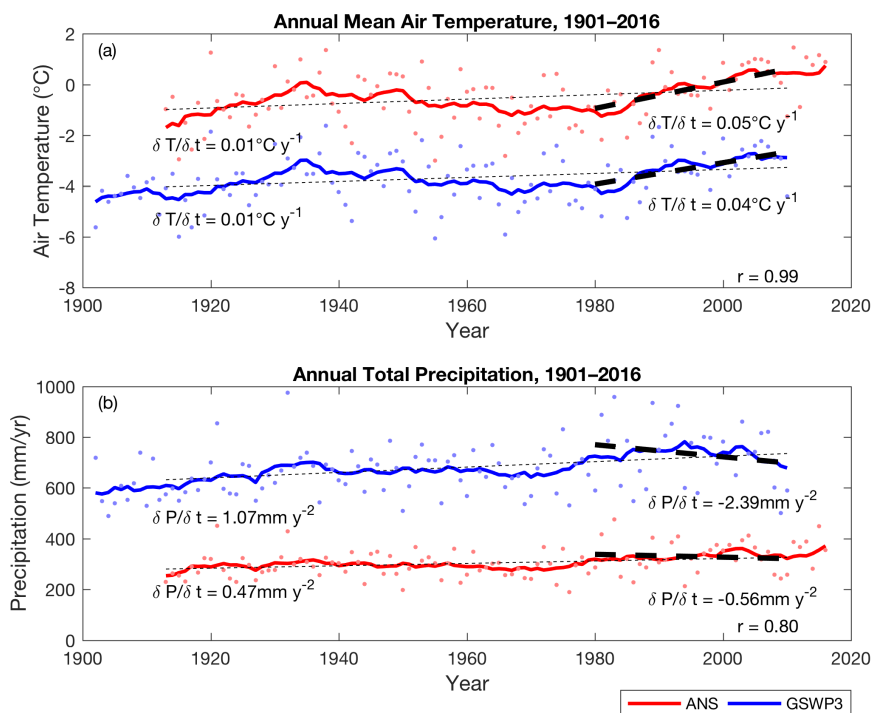


904 Table 3. Means and standard deviations of cumulative CO<sub>2</sub> and CH<sub>4</sub> exchanges simulated  
 905 at the palsa, bog, and fen sites during the period 2003 to 2007. All units are represented in  
 906 g C m<sup>-2</sup>.

Sites	C flux component	Growing season; Days 119–288		Non-growing season; Days 1–118/289–365	
		Mean	Standard deviation	Mean	Standard deviation
Palsa	CO <sub>2</sub>	-72.70	19.10	38.89	4.09
	CH <sub>4</sub>	0.04	0.02	0.01	0.002
Bog	CO <sub>2</sub>	-79.59	21.46	42.89	2.16
	CH <sub>4</sub>	3.52	0.45	0.42	0.11
Fen	CO <sub>2</sub>	-88.65	7.26	44.41	6.13
	CH <sub>4</sub>	10.86	3.95	0.78	0.18

907

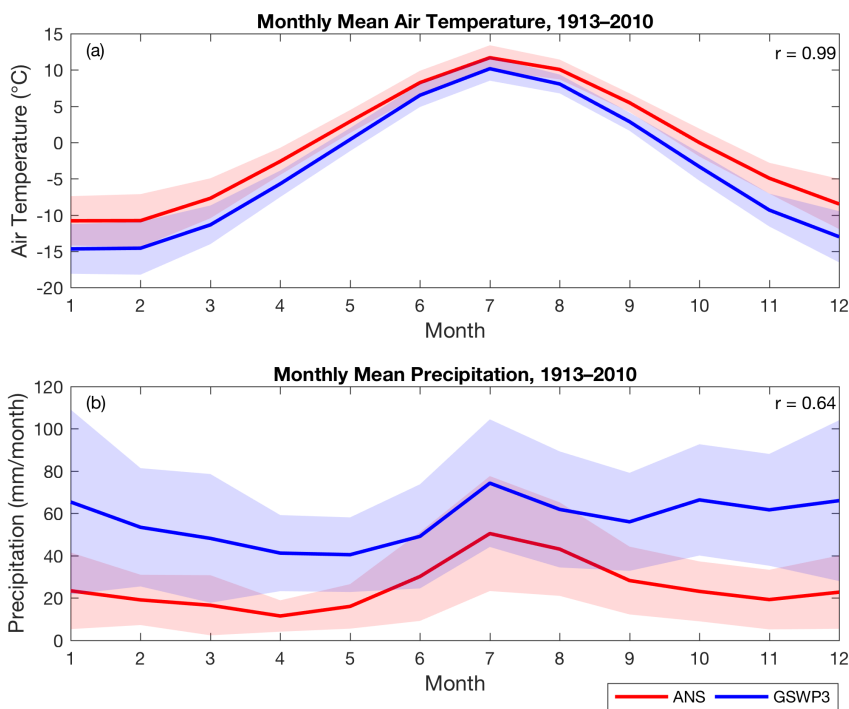
908



909

910 Figure 1. Time series of the air temperature (a) and precipitation (b) measured at ANS  
911 (red; years 1913–2016) and extracted from GSWP3 (blue; years 1901–2010). Dots are  
912 the annual means and solid lines are the decadal moving averages of the corresponding  
913 annual means. Thin and thick dashed lines are the trends for years 1913–2010, and years  
914 1980–2010, respectively. The inset  $r$  values are the correlation coefficients calculated  
915 between the two time series.

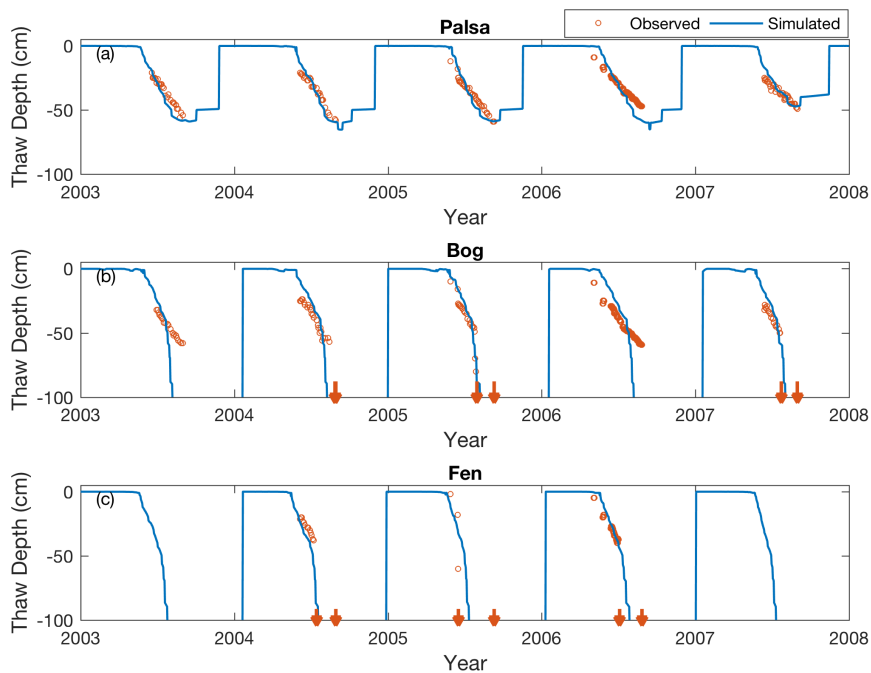
916



917

918 Figure 2. Monthly mean air temperature (a) and precipitation (b) measured at ANS (red)  
919 and extracted from GSWP3 (blue). The shaded area is the inter-annual variability for the  
920 corresponding dataset, represented by the standard deviations calculated at each month.  
921 The inset  $r$  values are the correlation coefficients calculated between the two time series.

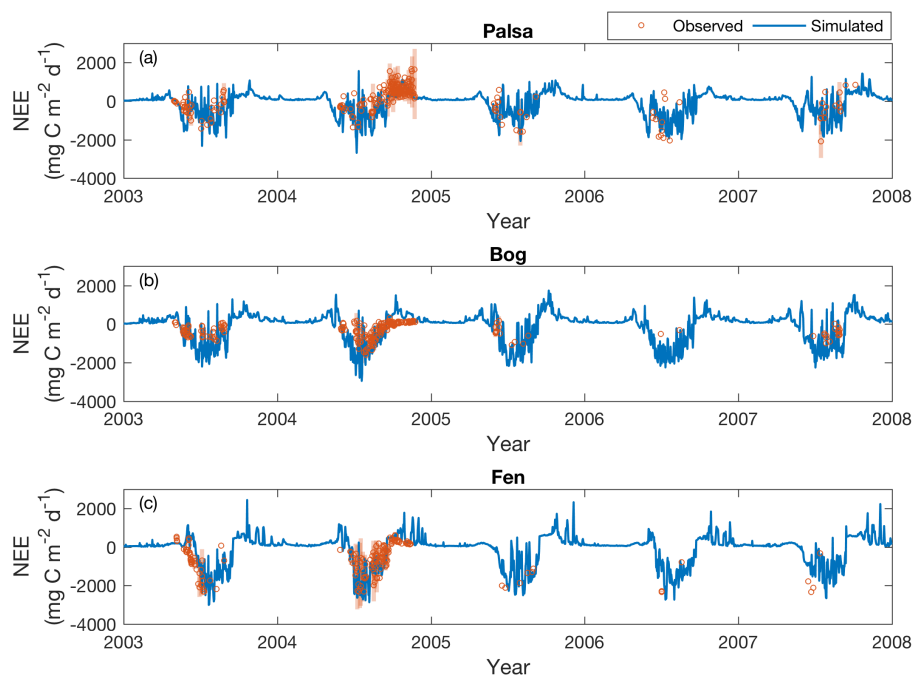
922



923

924 Figure 3. Simulated (solid lines) and measured (open circles) seasonal dynamics of thaw  
925 depth at the palsa (a), bog (b), and fen (c) sites from 2003 to 2007. Downward arrows  
926 indicate the time period that the measured thaw depth is deeper than 90 cm for a  
927 measurement year.

928



929

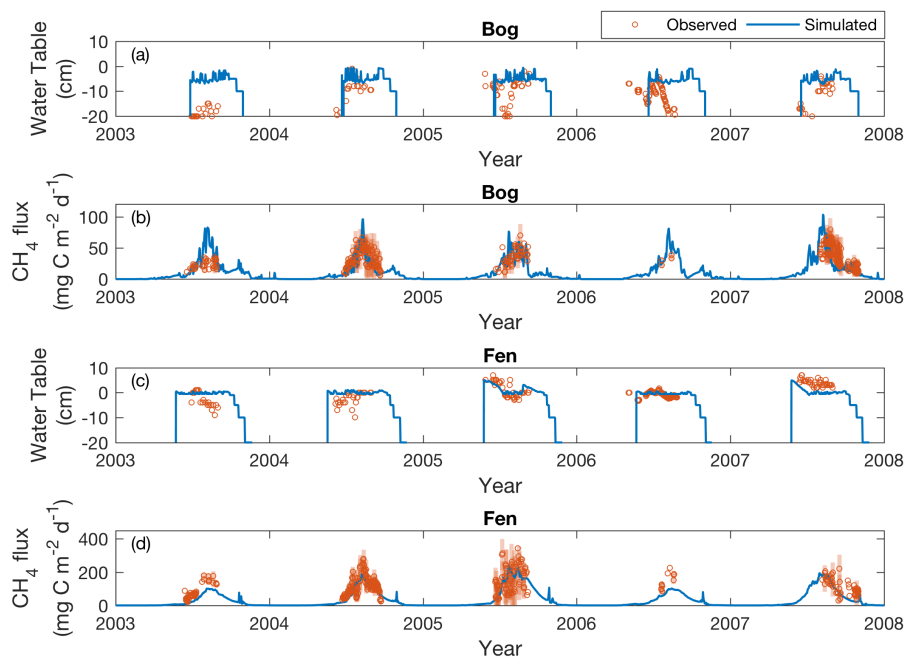
930 Figure 4. Simulated (solid lines) and measured (open circles) daily  $\text{CO}_2$  exchanges (NEE)

931 at the palsa (a), bog (b), and fen (c) sites, from 2003 to 2007. Shaded bars are the

932 standard deviations of the daily NEE measured across the subsites under each peatland

933 type. The positive values indicate effluxes, and the negative values indicate influxes.

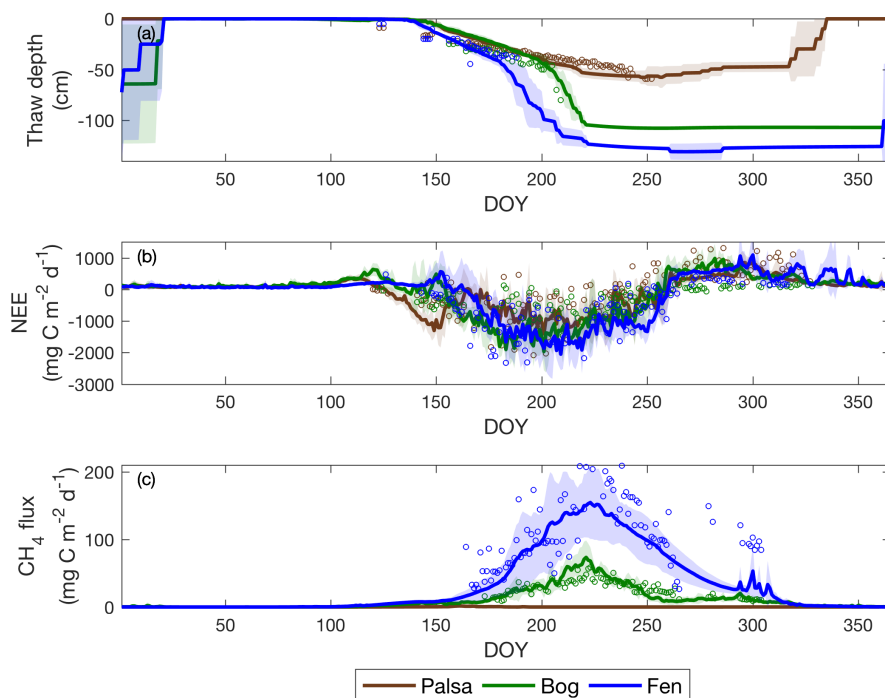
934



935

936 Figure 5. Simulated (solid lines) and measured (open circles) water table depth and daily  
937 CH<sub>4</sub> emissions at the bog and fen sites from 2003 to 2007. Shaded bars are the standard  
938 deviations of the daily CH<sub>4</sub> emissions measured across the subsites under each peatland  
939 type.

940



941

942 Figure 6. Daily composite results of (a) thaw depth, (b) daily NEE, and (c) daily CH<sub>4</sub>

943 exchanges across the thaw gradient from 2003 to 2007. Solid lines and open circles are

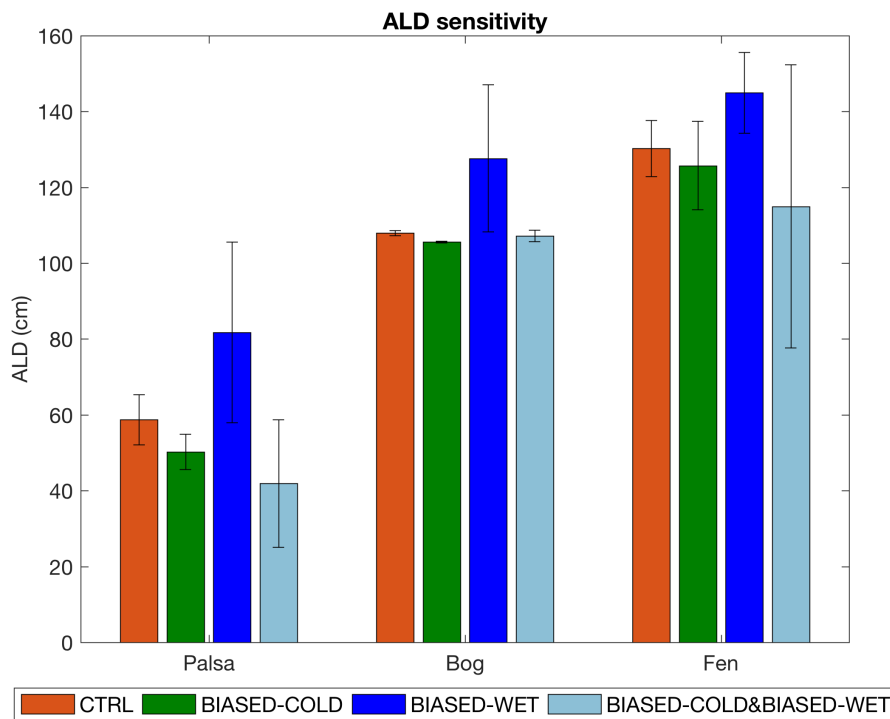
944 the simulated and measured inter-annual means, respectively. The shaded area is the

945 simulated inter-annual variability for the corresponding dataset, represented by the

946 standard deviations calculated at each day of year. The positive values indicate effluxes,

947 and the negative values indicate influxes.

948

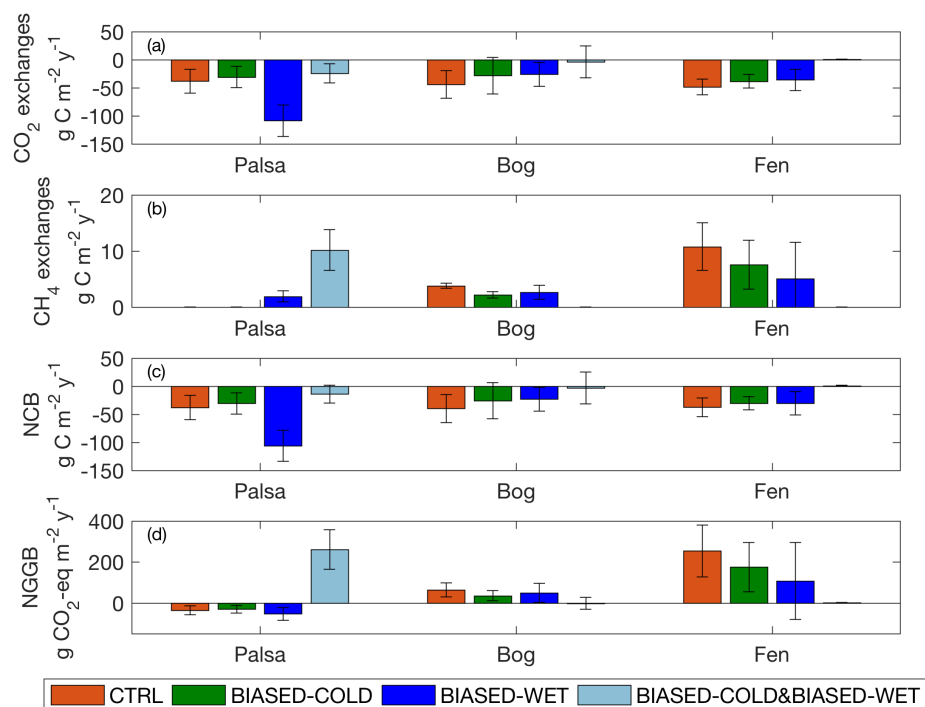


949

950 Figure 7. Simulated ALD at the palsa, bog, and fen sites, for four sets of climate forcing  
951 (Section 2.5). Bars and error bars are the means and standard deviations calculated from  
952 2003 to 2007, respectively.

953

954



955

956 Figure 8. Annual CO<sub>2</sub> exchanges (a), CH<sub>4</sub> exchanges (b), Net Carbon Balance (c), and  
 957 Net Greenhouse Gas Balance (d) simulated at the palsa, bog, and fen sites, under each set  
 958 of simulations. Bars and error bars are the means and standard deviations calculated from  
 959 2003 to 2007, respectively. The positive values indicate effluxes, and the negative values  
 960 indicate influxes.

961

962